JOURNAL OF CATALYSIS 112, 392–400 (1988)

Methane Activation over MoS_2 and CH_n Stabilities: Molecular Orbital Theory

ALFRED B. ANDERSON, JOHN J. MALONEY,[1] AND JENWEI YU

Chemistry Department, Case Western Reserve University, Cleveland, Ohio 44106

Received October 29, 1987; revised February 28, 1988

It is shown that four-fold coordinated Mo^{IV}, which is expected to be present at edges of MoS_2 plates, inserts into a methane CH bond to yield oxidative addition products. The H^- will transfer to S^{2-} and bind to it as H^+; the heterolytic adsorption products are more stable. Adsorbed CH_3 can dehydrogenate, yielding CH_2 doubly bonded to Mo but further dehydrogenations are destabilizing. It is concluded that in Fischer–Tropsch catalysis over MoS_2 adsorbed C and CH are short-lived and that chain propagation may involve adsorbed CH_2 and CH_3. These findings suggest that it may be possible to incorporate CH_4 in Fischer–Tropsch synthesis over MoS_2 and perhaps other catalysts.

INTRODUCTION

Recently we made a molecular orbital study of methane CH activation on several transition metal surfaces (*1*). Although some variations in activation energies were found for different metals (Fe, Ni, and Pt were studied) and different surface atom packing densities (bcc (110) and (100) and fcc (111) and (100) surfaces were examined), the transition state structures and orbital interactions were essentially the same. A single surface metal atom was found to insert into a CH bond and the bonding in the transition state was characterized by the metal stabilization of two C···H bonding molecular orbitals. The resulting lower energy one had three-centered C···H···*M* bonding and the upper one C···*M* bonding character. The lowest antibonding counterpart to these orbitals lay in the metal band and, due to participation of the C···H σ^*, H 1*s* contribution was eliminated and the orbital had C···*M* bonding character. These results are shown as schematically in Fig. 1. The surface metal atoms were more active toward a methane CH bond as the number of nearest neighbor metal atoms decreased. For the Fe surfaces, the "rough" one consisting of an Fe adatom on the (100) surface was most active and this atom was coordinated to only four nearest neighbors.

The metal surface results permit two interesting speculations. First, stabilization of the transition state should be primarily controlled by the degree of coordinative unsaturation of the metal center and not the number of *d* electrons or oxidation state. Whether or not the above-mentioned antibonding counterpart is occupied, activation should be strong. Second, if an environment can be found for a metal atom or cation in which the d_{xz} or d_z2 orbitals are relatively little involved in bonding, then these orbitals will be better able to activate CH bonds. The first point is supported by recent organometallic studies involving low coordination d^0 transition metal centers (*2*). Experimental evidence for the second point has yet to be developed, although it is generally believed that isolated metal atoms will be particularly reactive.

In this paper we examine methane CH activation on four-coordinate Mo^{IV} at the edge of an MoS_2 crystal. The atom superposition and electron delocalization molecular orbital (ASED-MO) theory is used. Such Mo^{IV} are at the apices of nearly square pyramids, bound to four S^{2-}, and the d_{xz}, d_{yz},

[1] Present address: Ferro Corp., Coatings Division, 4150 E. 56th Street, Cleveland, OH 44105.

0021-9517/88 $3.00

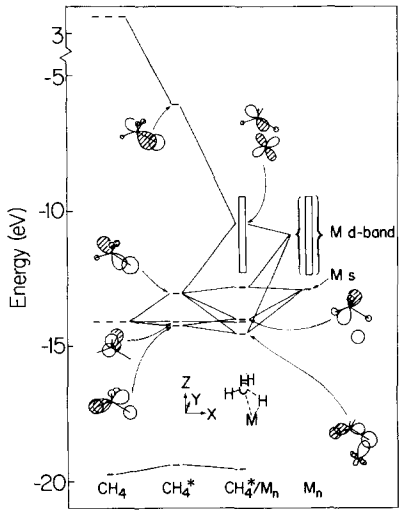

FIG. 1. Orbital interactions during insertion of an atom in a transition metal surface into a methane CH bond. The second column of energy levels is for CH_4 in the transition state structure with the surface cluster removed and the third is for the transition state on the metal surface.

and d_z2 orbitals should be relatively unencumbered by bond formation to S and hence are expected to lead to strong activity toward CH_4. In addition to CH activation, the binding of CH_3, CH_2, and CH fragments to this site and to S^{2-} is examined. In a previous ASED-MO study we calculated H adsorption properties on various Mo and S surface sites (*3*).

MoS_2 has an interesting layered structure. The easy cleavage between layers gives MoS_2 its solid-state lubricating property and the edges of the layers, where coordinatively unsaturated Mo is available, give it interesting catalytic properties. A cross section of a layer is shown in Fig. 2. Except at the edges, each Mo sits at the center of a triangular prism of S^{2-}. These S^{2-} make up the faces of each layer and account for the inertness and lubricating property of the layer surfaces.

Nothing exact is yet known about the structures of the edge sites. An ideal stoichiometric MoS_2 layer might terminate in edges with six-, four-, and two-fold coordinated Mo as shown for the case of the

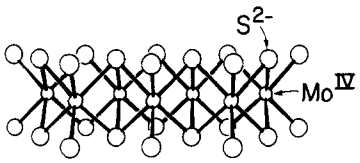

FIG. 2. Structure of a layer of MoS_2. Larger spheres are S^{2-}.

smallest possible hexagonal plate in Fig. 3. It is easily seen that in the macroscopic limit the ratio of numbers of six- to four- and two-fold edge Mo is 3 : 2 : 1 for this idealized structure. Such polar surfaces might be expected to form when layers are broken, just as occurs for other solids such as wurtzite-structured ZnO. Edge restructuring would be expected, especially for the two-fold edge. In the case of ZnO the cleaved polar surfaces consist of either three-fold coordinated Zn^{2+} or O^{2-}, each with one vacancy in the tetrahedral coordination. Relaxations of 0.35 Å for Zn^{2+} and 0.15 Å for O^{2-} have been calculated previously (*4*) using the ASED-MO theory and are within the ranges of experimental determinations using low-energy electron diffraction spectroscopy (*5*). It is likely, however, that the edges of MoS_2 are not simple polar ones but rather have Mo with various coordinations.

It was found in our study of H adsorption at edges (*3*), and also in an extended Hückel band calculation (*6*), that coor-

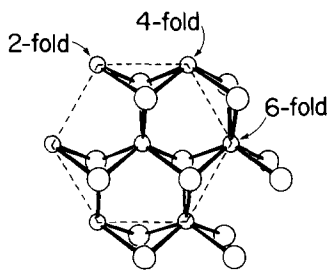

FIG. 3. Stoichiometric hexagonal Mo_7S_{14} plate of MoS_2. Larger spheres are S^{2-}. When MoS_2 units are aligned as shown, edge Mo^{IV} have six-, four-, and two-fold coordination. A dashed line outlines the hexagonal cation arrangement.

dinatively unsaturated edge Mo cations take some charge from the bulk-coordinated Mo^{IV}. The reason is easily understood. The bulk electronic structure has a filled S 3*p* band and at the top of it a filled *d* band. The other *d* bands are higher in energy and empty. Since the *d* band orbitals are antibonding between Mo and S, the removal of S ligands at a crystal edge reduces the antibonding destabilization and allows some *d* band orbitals to become stabilized so that they accept charge from bulk-coordinated Mo^{IV}. Surface state orbitals also appear in the bulk band gap.

Evidence for reduction of coordinatively unsaturated edge Mo^{IV} has been obtained recently by XPS and UPS (*7*). The edges were prepared by Ar ion etching around dispersed polystyrene spheres, followed by cleaning and reduction in H_2–H_2S to remove oxygen and resulfide. From XPS difference spectra, weak photoemission peaks associated with edge Mo 3*d* peaks were identified. The 0.8-eV shift to lower binding energy was used to assign them to Mo^{III}. Whether this is a result of nonstoichiometry in MoS_2 at the reduced edge sites, as suggested in Ref. (*7*), or the coordinatively unsaturated Mo which must be present even at edges of stoichiometric crystals, or both, is not known. If it is the latter, then careful examination of XPS difference spectra might reveal higher energy emissions due to Mo^{V} located just below the edge surfaces; it would be worthwhile to look for such emissions.

Chemical evidence for edge site coordinative unsaturation in MoS_2 catalysts is strong. H_2S adsorption blocks coordinatively unsaturated (it is assumed) edge sites toward hydrogenation and exchange of olefins (*8*). The presence of threefold coordinatively unsaturated Mo has been postulated for olefin hydrogenation and twofold coordinatively unsaturated sites for olefin isomerization (*9*). NO oxidizes edge but not basal plane Mo at 570 K (*10*) and dissociates at edges at temperatures as low as 130 K according to a study using polycrystalline samples (*11*). The adsorption of O_2 has also been associated with edge Mo (*10–12*), as has the adsorption of CO (*13*). Edge Mo are believed to be involved in hydrodesulfurizations (*14*) and are expected to play a role in Fischer–Tropsch catalysis (*15*). By contrast, the S^{2-}-covered basal planes are chemically inactive at ordinary temperatures toward thiophene, butene, H_2S (*16*), and O_2 (*17*).

METHOD AND MODELS

The atom superposition and electron delocalization molecular orbital theory used in this work may be understood as follows. Consider a diatomic molecule *ab* (this discussion is easily generalized to polyatomics). As separated noninteracting atoms, the electronic charge density distribution function for *ab* is the sum of the free atom functions ρ_a and ρ_b. These spherical functions are centered on and "follow" the nuclei "perfectly." When the atoms come together, a "non-perfectly-following" bond charge density distribution ρ_{npf} develops and the molecular density, ρ_{mol}, is then a sum of three components,

$$\rho_{mol} = \rho_a + \rho_b + \rho_{npf}. \quad (1)$$

Therefore, the force on one of the nuclei, say nucleus *b*, is the sum of the nuclear–nuclear repulsion force and the attractive forces due to ρ_a, ρ_b, and ρ_{npf}. The force due to ρ_b, which is centered on nucleus *b* is zero, the force due to atom *a* (its nucleus + electronic charge) is repulsive, and the force due to ρ_{npf} is attractive. These forces are integrated as the bond forms to give a binding energy *E* (*18*),

$$E = E_R + E_{npf}, \quad (2)$$

where E_R is the repulsive energy due to the interaction of nucleus *b* with atom *a* and E_{npf} is the attractive energy due to its interaction with ρ_{npf}:

$$E_R = Z_b(Z_a|R_a - R_b|^{-1} - \int \rho_a(\mathbf{r})|R_b - \mathbf{r}|^{-1}d\mathbf{r}) \quad (3)$$

$$E_{\text{npf}} = -Z_b \int_{\infty}^{R_b} \int \rho_{\text{npf}}(\mathbf{r},R_b') \times d/dR_b' |R_b' - \mathbf{r}|^{-1} d\mathbf{r} dR_b'. \quad (4)$$

E_R is calculated using an atomic density distribution function derived from valence atomic orbitals and E_{npf} is approximated (*19*) as the change in the total valence one-electron orbital energy which is due to bond formation,

$$E \simeq E_R + \Delta E_{MO}, \quad (5)$$

where

$$\Delta E_{MO} = \Sigma n_i \varepsilon_i^{ab} - \sum_a \sum_i n_i \varepsilon_i^a. \quad (6)$$

In Eq. (6), n_i are occupation numbers (0, 1, 2) and ε_i^{ab} are molecular orbital energies obtained by diagonalizing a Hamiltonian with matrix elements

$$H_{ii}^{aa} = \varepsilon_i^a = -\text{IP}_i^a \quad (7)$$

$$H_{ij}^{aa} = 0 \quad (8)$$

$$H_{ij} = 1.125(H_{ii}^{aa} + H_{jj}^{bb})S_{ij}\exp(-0.13R), \quad (9)$$

where IP_i^a is the i^{th} orbital ionization potential of atom a, $S_{ij} = \langle i,a|j,b\rangle$, and R is the internuclear distance. Complete details of the theory have been published recently (*20*). When this approximation to E_{npf} is used, the more electronegative atom is used to provide the density function for E_R. C and S have the same electronegativity so the C density and S nuclear charge are used in calculation C–S contributions to E_R because better results are obtained for the diatomic CS molecule when this is done than when the S density and C nucleus are used.

The atomic orbital parameters used in this study are in Table 1. They are taken from Ref. (*3*) except for C for which our standard C exponents are used and ionization potentials are increased 2.5 eV from the measured values (just as was done for H) so as to produce acceptable ionicity in MoC. Using bond length increments of 0.01 Å, results for diatomic fragments given in Table 2 are obtained. It is noted that the MoH bond strength is overestimated, the SH bond strength is accurate, and the CS bond strength is underestimated. In the present work CS single bonds are relevant. A calculation on CH_3SH yielded a CS single bond strength in agreement with experiment (2.5 eV) and a SH bond strength also in agreement with experiment (3.9 eV), but in both cases the bond lengths are overestimated by 0.2 Å.

Most of the calculations in this paper are on the edge site model shown in Fig. 4. This $Mo_7S_{22}^{16-}$ cluster has a fourfold coordinate edge Mo with a sixfold coordinate Mo on either side, in keeping with expectations for an edge of a stoichiometric plate as discussed in the Introduction. The 16- charge does not affect the Hamiltonian in ASED-MO calculations but establishes the proper number of electrons for modeling bulk

TABLE 1

Parameters Used in the Calculations: Principal Quantum number, n, Orbital Ionization Potential, IP (eV), Slater Orbital Exponents, ζ (a.u.), and Corresponding Linear Coefficients, c^a

Atom	s			p			d					
	n	IP	ζ	n	IP	ζ	n	IP	ζ_1	ζ_2	c_1	c_2
H	1	11.1	1.2									
C	2	14.09	1.658	2	8.76	1.618						
S	3	19.50	2.022	3	9.66	1.727						
Mo	5	7.80	1.956	5	4.62	1.656	4	9.26	4.542	1.701	0.60814	0.60814

[a] Except for C (see text), these are from Ref. (*3*).

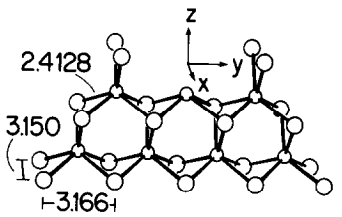

FIG. 4. Cluster model of twofold coordinatively unsaturated edge Mo^{IV} surrounded by two sixfold coordinated edge Mo^{IV}. The nearest-neighbor MoS distances are all the same (Å). Structure data from "Structure Reports" (W. B. Pearson, Ed.), Vol. 19. International Union of Crystallography, Utrecht, 1964.

MoS_2 with this cluster. Some tests of MoS bonding were made using this and a $Mo_7S_{24}^{20-}$ hexagonal cluster of the form of Fig. 3 but with bulk-coordinated edge Mo^{IV}. A fully coordinated S^{2-} on the basal plane of the latter cluster was calculated to relax away from the Mo^{IV} plane by 0.09 Å so that the MoS distances increased from the 2.41-Å experimental value to 2.50 Å. This 0.09-Å increase is an error due to the approximate nature of the ASED-MO theory. A small (~0.1 a.u.) increase in the S valence exponents would eliminate this error but would not affect our other conclusions. Interestingly, when edge sulfur pairs are relaxed (in this case a pair was added to the fourfold coordinated Mo of Fig. 4 and all three pairs along this edge were relaxed) the MoS bonds stretch to 2.90 and the SMoS angle decreases from 81.5 to 77°. There are two contributing factors, based on Mulliken overlap analysis, to this unexpectedly large stretch. First, within a surface the nearest-neighbor S–S overlaps are negative, indicating a net closed-shell S^{2-}–S^{2-} repulsive interaction, and stretching relieves this. Second, MoS overlaps adjacent to the edges increase as a result of stretching, indicating that these bonds are strengthening. In another probe of the edge model, the four-coordinate Mo^{IV} was relaxed along the direction of the z axis, and was calculated to move 0.19 Å away from the edge, which corresponds to a Mo–S bond stretch of 0.08 Å. This suggests that edge Mo relaxations will be small. For simplicity, we maintain bulk superimposability for the cluster models of MoS_2. Reported angles are optimized in 1° steps and bond lengths in 0.01-Å steps. The CH_3 group is fixed rigidly in the methane structure.

TABLE 2

Calculated and Experimental or Estimated (Parentheses) Diatomic Bond Length, R_e (Å), Force Constant, k_e (mdyn/Å), and Dissociation Energy, D_e (cV) for Diatomic Molecules Using the Surface-Adapted Parameters in Table 1

Molecule	State	R_e	k_e	D_e
MoC	$^5\Sigma$	1.82 (~1.65)[a]	7.0	5.0 (7.0)[a]
MoH	$^6\Sigma$	1.71 (~1.68)[a]	2.5	3.6 (2.2)[b]
MoS	$^5\pi$	2.26 (~2.20)[a]	3.2	3.2 (~3.7)[a]
CS	$^1\Sigma$	1.64 (1.53)[c]	6.4 (8.49)[c]	5.3 (7.43)[c]
SH	$^2\pi$	1.53 (1.34)[c]	2.5 (4.23)[c]	3.7 (3.7)[c]

[a] Extrapolated from known values of other diatomic molecules given in footnote [c].

[b] Experimental value from L. Sallans, K. R. Lane, R. R. Squires, and B. S. Freisen, *J. Amer. Chem. Soc.* **107,** 4379 (1985).

[c] Experimental value from K. P. Huber and G. Herzberg, "Constants of Diatomic Molecules." Van Nostrand–Reinhold, New York, 1979.

CH_4 ACTIVATION

An activation energy barrier of 0.21 eV (20 kJ/mol) is calculated for methane CH activation, indicating that the four-coordinate edge Mo^{IV} should be very active. The transition state structure is in Fig. 5 and is

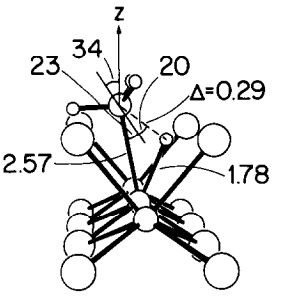

FIG. 5. Calculated transition state structure for four-coordinate edge Mo^{IV} inserting into a methane CH bond; (Å and °). The angles labeled 20 and 23 are with respect to the tetrahedral direction through C.

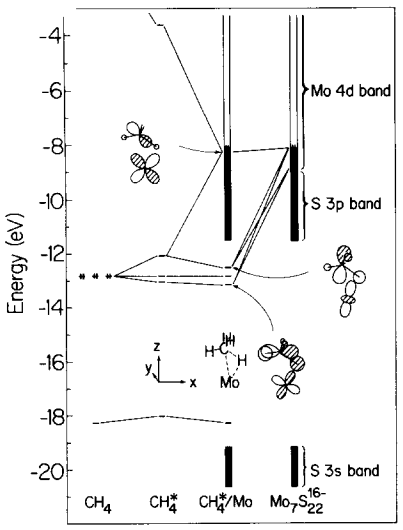

FIG. 6. Orbital interactions during insertion of an edge four-coordinated Mo^{IV} into a methane CH bond. The second column of energy levels is for CH_4 in the transition state structure with the sulfide cluster removed and the third is for the transition state over the Mo^{IV}.

remarkably similar to those obtained on metal surfaces in Ref. (*1*). As expected, the d_z2 and d_{xz} orbitals of the activating Mo^{IV} participate—see Fig. 6. Of the orbitals drawn, the lowest is the same type of three-centered C···H···*M* interaction as that seen for the metal surfaces. The next one has C···*M* bonding as well as *M*···H and C···H bonding. The first antibonding counterpart to these C···H σ donation bonds to Mo^{IV} loses most of the H 1*s* contribution because of C···H σ^* participation, and is essentially nonbonding between C and Mo. The total change in two-body E_R contributions to the activation energy is 0.24 eV. Because this is small compared to a bond strength, the activation of CH by the Mo can be viewed simply as an orbital result.

Since the four-coordinate Mo^{IV} is at the apex of a pyramid that is close to being square, with a base measuring 3.150 × 3.166 Å, the d_{yz} orbitals should be just as available for activating the CH bond as the d_{xz} orbital. To test this, we removed the four S^{2-} that surrounded the original four-coordinate Mo^{IV} site to eliminate the steric crowding which would accompany rotating the $H_3C\cdots H$ system. The resulting $Mo_7S_{18}^{8-}$ cluster has three four-coordinate Mo^{IV} lined up in a row. Using the same structure for the transition state as above, the activation energy becomes 0.37 eV. Maintaining the structure and rotating 90°, one changes the activation energy to 0.41 eV. This means that the d_{yz} orbital is nearly as effective as the d_{xz} orbital in the four-coordinate edge Mo^{IV}. This being the case, an intermediate rotation, which would hybridize the d_{xz} and d_{yz} orbitals, should also show activation. At 45° the activation energy is 0.45 eV, which is close to the previous values.

ACTIVATION PRODUCT STABILITIES

The immediate products of the insertion reaction are H^- and CH_3^- bound to Mo^{VI} as shown in Fig. 7. The calculations produce an exothermicity of 1.0 eV. Since the MoH bond strength may be overestimated and the MoC bond strength may be underestimated (Table 2), this exothermicity should be of the proper magnitude, but may be high. The σ bonding of these fragments adsorbed independently on edge Mo^{IV} sites is shown in Fig. 8.

We approached the question whether these insertion products might rearrange the heterolytic products, as anticipated from the earlier study of H_2 (*3*) and studies of CH_4 on metal oxides where heterolytically adsorbed products were found most stable (*21*), by examining the adsorption of H and CH_3 independently on edge Mo^{IV} and

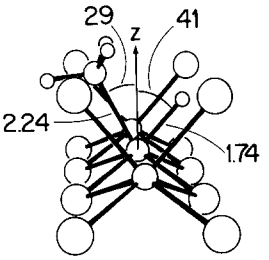

FIG. 7. Structure of oxidative addition products.

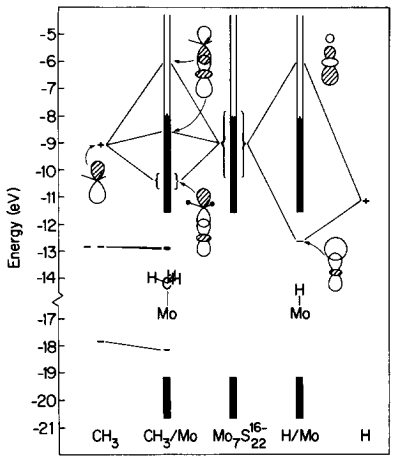

FIG. 8. Orbital correlation diagram for CH_3 and H binding to edge four-coordinate Mo^{IV}.

S^{2-} and basal plane S^{2-}. Adsorption energies and structures are given in Table 3. The H adsorption energy on the basal plane S^{2-} is 2.65 eV and on the edge Mo^{IV} it is 4.23 eV. Since we expect the correct MoH bond strength to be less, in the range 2.2 to 3.1 eV (*3*), it is probable that H will be able to shift from Mo to S, resulting in heterolytic products. If CH_3 were to shift to S^{2-}, it would destabilize the system by 1.0 eV, according to the calculations, which will retard the formation of reductive homolytic products. The weakness of CH_3 adsorption on basal plane S^{2-} when compared with the

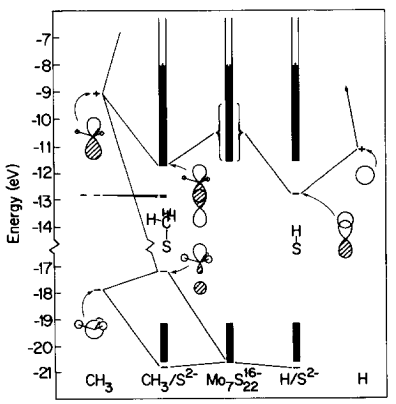

FIG. 9. Orbital correlation diagram for CH_3 and H binding to basal plane S^{2-}.

TABLE 3

Calculated Bond Lengths (Å), Angles (°), and Adsorption energies E (eV) for Fragments on MoS_2 Using the Cluster in Fig. 4

Fragment	Site	Distance	E
H	Edge Mo	1.73	4.36
H	Edge S	1.49	2.57
H	Basal S	1.46	2.65
CH_3	Edge Mo, along z axis	2.17	2.55
CH_3	Edge Mo, along MoS axis	2.24	1.91
CH_3	Edge S, 105 from z	2.06	1.23
CH_3	Basal S	1.95	1.55
CH_2[a]	Edge Mo, Fig. 10	1.97	4.94
CH_2	Edge Mo, rotated 90	2.00	4.23
CH[b]	Edge Mo	1.83	5.45
C	Edge Mo	1.84	5.93

Note. In CH_3, CH distances are fixed at 1.21 Å.

[a] CH distance decreases 0.02 Å from methyl values; HCH angle is 114°.

[b] CH distance decreases 0.04 Å from methyl value.

SC single bond strength of 2.5 eV is in part a result of the antibonding counterpart to the σ bond which promotes an electron to the lowest unoccupied molecular orbital as shown in Fig. 9. It is noted that the heterolytic products CH_3^+ on S^{2-} and H^- on Mo^{IV} are unstable. A similar electron promotion contributes to the calculated weakening of the SH bond on the basal plane by 1.2 eV from the diatomic SH value.

CH_2 AND CH AND C ADSORPTION

Methylene, CH_2, binds most strongly to a four-coordinate edge Mo^{IV} as shown in Fig. 10. The C forms a double bond to Mo^{IV}, making use of the d_z2 and d_{xz} orbitals as shown in Fig. 11. The energy change for the reaction of CH_3 on the four-coordinate edge

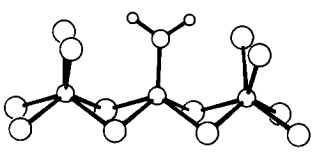

FIG. 10. Structure of CH_2 on an edge four-coordinate Mo^{IV}.

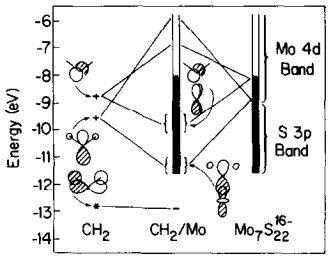

FIG. 11. Orbital correlations for the binding of CH_2 to Mo^{IV} in the structure of Fig. 10.

Mo^{IV} to yield CH_2 on this site and H on a basal plane S^{2-} is 0.12 eV (the result is nearly the same for an edge S^{2-}), implying a reversibility that is consistent with the Fischer–Tropsch activity of MoS_2. Rotation of CH_2 by 90° to cause double bonding using the d_{yz} orbital still allows strong double bonding, but with a 0.71 eV decrease in strength.

A strong triple bond forms between CH and the fourfold coordinated edge Mo^{IV}. To form this by dehydrogenation of CH_2, placing H on a basal plane S^{2-}, costs 0.60 eV. Consequently, further dehydrogenation of CH_2 is unlikely. A similar reaction of CH is destabilizing by 1.35 eV. However, CH and C will be readily hydrogenated, which is in agreement with the Fischer–Tropsch activity of MoS_2.

CONCLUSIONS

Not only will fourfold coordinated Mo^{IV} be active toward CH_4, but so will three- and twofold coordinated Mo^{IV} because they too will have two d orbitals available to stabilize the transition state and to form Mo–H and Mo–CH_3 bonds. The activity predicted by the calculations in this study is, based on analysis of the bonding in the transition states, independent of the actual oxidation state of Mo. The presence of low oxidation states of Mo (<4) in the MoS_2 catalyst is symptomatic of relatively high coordinative unsaturation and therefore high activity, but our theoretical bonding analysis shows that even d^0 Mo^{VI} might activate CH_4 if it has sufficient coordinative unsaturation.

Our study also bears on Fischer–Tropsch catalysis by MoS_2 (*15*). In other work (*22*) we have shown that early transition metal atoms and cations, which are d electron deficient, activate CO because CO can form a strong π donation bond to such centers wherein the O end of the molecule also binds to the metal. When thereby coordinated through both C and O, 5σ donation is also enhanced and so is d–π^* back-donation. The result is a weak CO bond which dissociates easily, forming adsorbed C at coordinatively unsaturated edge sites. Using the sites discussed above, with C bonded to the edge fourfold coordinated Mo^{IV} and H bonded to corner or basal plane S^{2-}, we can write

$$C_{(ads)} + H_{(ads)} \rightarrow CH_{(ads)}$$

$$CH_{(ads)} + H_{(ads)} \rightarrow CH_{2(ads)}$$

$$CH_{2(ads)} + H_{(ads)} \leftrightarrows CH_{3(ads)}$$

$$CH_{3(ads)} + H_{(ads)} \leftrightarrows CH_{4(g)}$$

These reactions indicate that if C and CH intermediates form during Fischer–Tropsch synthesis of C_n hydrocarbons they will be short-lived; CH_2 and CH_3 are the C_1 intermediates of importance in building long-chain hydrocarbons. Preliminary calculations using a row of edge fourfold coordinate Mo^{IV} show CH_3 and CH_2 are the more mobile species. Another possibility is CO insertion into the Mo-CH_3 bond and subsequent hydrogenation, as discussed by Klier and coworkers (*23*). We are presently studying these mechanisms.

From the above, it seems worthwhile to try to incorporate methane in the Fischer–Tropsch reactions over MoS_2. Other Fischer–Tropsch catalysts might also be effective.

ACKNOWLEDGMENT

We are grateful for the support of the Gas Research Institute, which made this work possible.

REFERENCES

1. Anderson, A. B., and Maloney, J. J., *J. Phys. Chem.* **92**, 809 (1988).

2. Thompson, M. E., Baxter, S. M., Bulls, A. R., Burger, B. J., Nolan, M. C., Santarsiero, B. D., Schaefer, W. P., and Bercaw, J. E., *J. Amer. Chem. Soc.* **109,** 203 (1987).
3. Anderson, A. B., Al Saigh, Z. Y., and Hall, W. K., *J. Phys. Chem.* **92,** 803 (1988).
4. Anderson, A. B., and Nichols, J. A., *J. Amer. Chem. Soc.* **108,** 1385 (1986).
5. Gay, R. R., Nodine, M. H., Henrich, V. E., Zieger, H. J., and Solomon, E. I., *J. Amer. Chem. Soc.* **102,** 6752 (1980).
6. Zonnevylle, M. C., Hoffmann, R., and Harris, S., in press.
7. Roxlo, C. B., Deckman, H. W., Gland, J., Cameron, S. D., and Chianelli, R. R., *Science* **235,** 1629 (1987).
8. Okuhara, T., Tanaka, K., and Miyahara, K., *J. Catal.* **48,** 229 (1977).
9. Tanaka, K., and Okuhara, T., *J. Catal.* **78,** 155 (1982).
10. Susuki, K., Soma, M., Onishi, T., and Tamaru, K., *J. Electron Spectrosc. Relat. Phenom.* **24,** 283 (1981).
11. Shuxian, Z., Hall, W. K., Ertl, G., and Knözinger, H., *J. Catal.* **100,** 167 (1986).
12. Valyon, J., and Hall, W. K., *J. Catal.* **84,** 216 (1983).
13. Peri, J. B., *J. Phys. Chem.* **86,** 1615 (1982).
14. Topsoe, H., and Clausen, B. S., *Catal. Rev. Sci. Eng.* **26,** 395 (1984).
15. Dianis, W. P., *Appl. Catal.* **30,** 99 (1987).
16. Salmeron, M., Somorjai, G. A., Wold, A., Chianelli, R., and Liang, K. S., *Chem. Phys. Lett.* **90,** 105 (1982).
17. Farias, M. H., Gellman, A. J., Somorjai, G. A., Chianelli, R. R., and Liang, K. S., *Surf. Sci.* **140,** 181 (1984).
18. Anderson, A. B., *J. Chem. Phys.* **60,** 2477 (1974).
19. Anderson, A. B., *J. Chem. Phys.* **62,** 1187 (1975).
20. Anderson, A. B., Grimes, R. W., and Hong, S. Y., *J. Phys. Chem.* **91,** 4245 (1987).
21. Mehandru, S. P., Anderson, A. B., Brazdil, J. F., and Grasselli, R. K., *J. Phys. Chem.* **91,** 2930 (1987).
22. Anderson, A. B., and Dowd, D. Q., *J. Phys. Chem.* **91,** 869 (1987).
23. Santiesteban, J. G., Bogdan, C. E., Herman, R. G., Nunan, J. G., and Klier, K., Proc. 9th Intern. Congr. Catal., Calgary, Canada (1988), in press.